Analysing Performance Bounds for Direction of Arrival Based Localisation from Quantised Samples

Shaunak Kubal
dr. ing. Anastasia Lavrenko[†], prof. dr. ir. André Kokkeler[†], dr. ir. Pieter-Tjerk de Boer[††]
[†]Co-supervisor, [††]External committee member
B.Sc. Thesis, Faculty of EEMCS, University of Twente

***Abstract*—The fields of direction of arrival (DOA) estimation and localisation comprise of determining the position of a signal source, such as a radio frequency emitter or wireless communication device. These sources are measured, and their DOAs are determined by analysing properties such as phase differences. The location of the signal sources is then deduced using the DOAs at various observation points. Furthermore, these measurements are conducted using antenna arrays that record noise, necessitating that the problems of angle estimation and localisation be approached as statistical estimation problems. These statistical estimation problems can be analysed using theoretical performance metrics such as the Cramér-Rao lower bound (CRLB) and by formulating maximum likelihood estimation procedures.**

It is often advantageous to consider quantisation of the measured signal, as it offers practical benefits such as reduced data storage and processing requirements. However, quantisation makes the estimation problem more complex. This thesis presents a comprehensive derivation of the CRLB for the sub-problem of DOA estimation and, through this, the CRLB for localisation for both the non-quantised and 1-bit quantised cases. Key findings confirm that the CRLB in the 1-bit quantised case is lower bounded by the CRLB of the non-quantised case. Finally, maximum likelihood schemes are implemented and validate the attained lower bounds.

***Index Terms*—DOA estimation, localisation, Cramér-Rao lower bound (CRLB), maximum likelihood, quantisation.**

I. Introduction

Localisation [1] involves determining the location of some signal source within a defined spatial environment. Examples include identifying the position of cellular phone signals, GPS transmitters, radio frequency identification (RFID) tags, or radar sources. One of the standard methods of localisation involves determining the position of the source by utilising the angles formed between the signal source and predetermined positions, such as antenna arrays, within the environment [1]. Such an angle, also known as the direction of arrival (DOA), can be inferred by measuring the signal at the antenna array and recording the signal phase differences at their elements [2]. In a realistic setting, these antenna arrays also capture noise, which introduces some variance into the deduced angle, thereby making the deduction of the DOA a statistical estimation problem. Given this, the precision of estimating the DOA is bounded by the Cramér-Rao lower bound (CRLB) [3]. Here, the CRLB serves as a performance benchmark for estimation schemes of the DOA.

Localisation of the source signal is now achieved through DOA estimates, enabling the establishment of a CRLB for localisation precision as done in [1].

Implementing signal quantisation offers several advantages in practical applications, e.g., it reduces the amount of data that needs to be stored and processed, leading to more efficient use of computational resources. When applied to DOA estimation and localisation, quantisation is particularly feasible as it pertains directly to the received signal rather than any encoded data within the signal.

Previous studies, such as [4], extensively explore quantisation in parametric estimation, while works such as [2], [5] specifically focus on 1-bit quantisation for DOA estimation. Although [1] delves into localisation using DOA estimates and establishes a CRLB, it does not address the aspect of quantisation. This study aims to fill this gap by investigating the performance of estimation schemes for localisation using 1-bit quantised signal samples.

The report begins with establishing the sub-problem of DOA estimation and derives the CRLB for the cases of receiving a full-precision and 1-bit quantised source signal. Here, a comparison between the two CRLBs highlight the effect of quantisation on DOA estimation. Furthermore, the report uses the derived DOA CRLBs as the variance of DOA estimates in [1] to establish a more practical bound when compared to the one in [1]. Lastly, the report directly derives localisation CRLBs using non-quantised and quantised source signal samples as opposed to using DOA estimates, resulting in a true precision lower bound in a practical setting.

Note, several statistical terms used in this investigation are defined in explained in Appendix A.

II. DOA Estimation without Quantisation

A. Antenna Array Model

This investigation considers a uniform linear array (ULA) antenna model. This model consists of M uniformly spaced antenna elements, each capable of receiving an RF signal. The source is assumed to be a real cosine signal of constant amplitude and frequency defined as follows,

$$s(t) = A_0 \cos(\omega t).$$

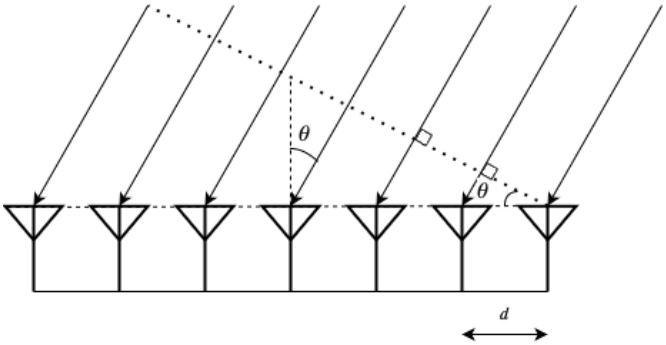

Fig. 1. Uniform linear array (ULA) model for direction of arrival estimation.

Here, A_0 is the signal amplitude and ω is the angular frequency. The ULA model operates under the far-field assumption that the distance between the source and the array is significantly greater than the spacing between the elements. As a result, the source travels an additional distance of $d\sin\theta$ at each successive antenna element, with θ representing the DOA, as evidenced by Fig. 1. Hence, the phase difference in the source observed between two successive elements is given by

$$\Delta\phi = \frac{2\pi}{\lambda} d\sin\theta. \tag{1}$$

Here, λ represents the source signal's wavelength. On choosing $d = \lambda/2$, the phase difference at any element m with respect to signal observed at the first element ($m = 1$) is given by

$$\phi_m(\theta) = (m-1)\pi\sin\theta. \tag{2}$$

Therefore, if the signal observed at $m = 1$ is $s(t)$, the signal observed at $m = k$ is $s(t + \phi_k(\theta))$. Here, the parameter θ is encoded within the phase of the received signal.

It should be noted that a drawback of the ULA model is its limitation in differentiating only within an angular range of π, specifically $(-\pi/2, \pi/2)$. For example, $-\pi$ would be indistinguishable from 0.

B. Received Signal Model

The antenna elements 'spatially' sample the time-dependent source signal. One could choose to observe a single temporal sample at each element; however, for practicality (and potentially better estimation), this investigation assumes the signal has been observed over a specific duration. Therefore, the received deterministic signal model is given by

$$x[n] = s(\omega n T_s) = A_0\cos(\omega n T_s) = A_0\cos(\Omega n)$$

Here, $\Omega = \omega T_s$ is the discrete angular frequency and n represents the temporal sample number. Thus, the deterministic array output is given by

$$\boldsymbol{x}[n] = \begin{bmatrix} A_0\cos(\Omega n) \\ \vdots \\ A_0\cos(\Omega n + \phi_M(\theta)) \end{bmatrix} \in \mathbb{R}^M, \;\; n = 1, \ldots, N. \tag{3}$$

The model is completed with the signal polluted with additive random noise at each antenna element and each time sample, resulting in the complete observed random sample. Therefore, the observed samples are given by

$$\boldsymbol{Y}[n] = \boldsymbol{x}[n] + \boldsymbol{e}[n] \in \mathbb{R}^M, \;\; n = 1, 2, \ldots, N. \tag{4}$$

This investigation assumes $\boldsymbol{e}[n]$ to be AWGN $\sim\mathcal{N}(\boldsymbol{0}, \boldsymbol{\Sigma})$, $\boldsymbol{\Sigma} = \sigma^2\mathbb{1}$ with a known σ^2, implying $\boldsymbol{e}$ is a spatially independent Gaussian random vector. Furthermore, $\boldsymbol{e}[n]$ are N i.i.d. random vectors. Therefore,

$$\boldsymbol{Y}[n] \sim \mathcal{N}(\boldsymbol{x}[n], \boldsymbol{\Sigma}) \tag{5}$$

so that $\boldsymbol{Y}[n]$ are independent but non-identical Gaussian random vectors. The expression in Eq. (4) can be interpreted as observing N random vectors in $\mathbb{R}^M$. Equivalently, one can concatenate each time sample into a tall vector and interpret it as observing one sample in $\mathbb{R}^{NM}$. By extension, it is valid to interpret the expression as observing $N \cdot M$ scalar samples with an underlying joint distribution.

C. Likelihood & Log-likelihood Functions

The probability density function (PDF) of $\boldsymbol{Y}[n]$ for a single time sample is given by,

$$f(\boldsymbol{y}[n]; \theta) = \det(2\pi\boldsymbol{\Sigma})^{-\frac{1}{2}} \exp\left(-\frac{1}{2}\langle \boldsymbol{y}[n] - \boldsymbol{x}[n], \boldsymbol{\Sigma}^{-1}(\boldsymbol{y}[n] - \boldsymbol{x}[n])\rangle\right). \tag{6}$$

Considering N temporal samples, the likelihood function is the joint density of all N independent random vectors (see Appendix A).

$$L((\boldsymbol{Y}[n])_{n=1}^N; \theta) = \prod_{n=1}^N \det(2\pi\boldsymbol{\Sigma})^{-\frac{1}{2}} \exp\left(-\frac{1}{2}\langle \boldsymbol{Y}[n] - \boldsymbol{x}[n], \boldsymbol{\Sigma}^{-1}(\boldsymbol{Y}[n] - \boldsymbol{x}[n])\rangle\right)$$

The log-likelihood function (see Appendix A) is obtained by taking $\ln(\cdot)$ on both sides, converting the product term into a sum term.

$$l((\boldsymbol{Y}[n])_{n=1}^N; \theta) = N\ln\left(\det(2\pi\boldsymbol{\Sigma})^{-\frac{1}{2}}\right) + \sum_{n=1}^N -\frac{1}{2}\langle \boldsymbol{Y}[n] - \boldsymbol{x}[n], \boldsymbol{\Sigma}^{-1}(\boldsymbol{Y}[n] - \boldsymbol{x}[n])\rangle. \tag{7}$$

The expression above can be further simplified by recognising that $\boldsymbol{\Sigma}^{-1}$ is a diagonal matrix with each element on the diagonal being $1/\sigma^2$. Pulling the noise variance term outside the inner product results in term $\|\boldsymbol{Y}[n] - \boldsymbol{x}[n]\|^2$ remaining in the summation, where $\|\cdot\|$ is the norm on $\mathbb{R}^M$. Expressing this term element-wise results in the following final expression

$$l((\boldsymbol{Y}[n])_{n=1}^N; \theta) = -\frac{N}{2}\ln\left(\det(2\pi\boldsymbol{\Sigma})\right) - \frac{1}{2\sigma^2}\sum_{n=1}^N\sum_{m=1}^M \left(Y_m[n] - A_0\cos(\Omega n + \phi_m(\theta))\right)^2. \tag{8}$$

D. Fisher Information & CRLB

The Fisher information, as defined in Appendix A, quantifies the amount of information that an observed sample carries about the unknown parameter. It is given by

$$\mathcal{J}(\theta) = \mathbb{E}\left[\left(\frac{\partial}{\partial\theta} l\left((\boldsymbol{Y}[n])_{n=1}^{N};\theta\right)\right)^2\right].$$

It can be proven that

$$\mathbb{E}\left[\left(\frac{\partial}{\partial\theta} l\left((\boldsymbol{Y}[n])_{n=1}^{N};\theta\right)\right)\right] = 0. \tag{9}$$

Therefore, the Fisher information simplifies to

$$\mathcal{J}(\theta) = \mathrm{Var}\left[\left(\frac{\partial}{\partial\theta} l\left((\boldsymbol{Y}[n])_{n=1}^{N};\theta\right)\right)\right]. \tag{10}$$

Recall the noise $\boldsymbol{e}$ is both spatially and temporally independent, implying that the $\mathrm{Var}(\cdot)$ produces no covariance terms. Therefore,

$$\begin{aligned}\mathcal{J}(\theta) = \sum_{n=1}^{N}\sum_{m=1}^{M} \mathrm{Var}\Big(&-Y_m[n](m-1)\pi\frac{A_0}{\sigma^2}\\ &\sin(\Omega n + (m-1)\pi\sin\theta)\cos\theta\\ &+ (m-1)\pi\frac{A_0^2}{\sigma^2}\cos(\Omega n + (m-1)\pi\sin\theta)\\ &\sin(\Omega n + (m-1)\pi\sin\theta)\cos\theta\Big).\end{aligned} \tag{11}$$

Evaluating the $\mathrm{Var}(\cdot)$ operator results in the following expression for the Fisher information,

$$\begin{aligned}\mathcal{J}(\theta) = \sum_{n=1}^{N}\sum_{m=1}^{M} \pi^2\frac{A_0^2}{\sigma^2}(m-1)^2\\ \sin^2(\Omega n + (m-1)\pi\sin\theta)\cos^2\theta.\end{aligned} \tag{12}$$

Finally, the CRLB (see Appendix A) given by

$$\mathrm{CRLB}(\theta) = \frac{1}{\mathcal{J}(\theta)}, \tag{13}$$

serves as both a performance metric and a theoretical performance limit for all unbiased estimators of the parameter θ.

E. Results & Discussion

The plot in Fig. 2 shows the obtained CRLB as a function of the parameter θ for different noise variances (noise powers). Fig. 2 shows two prominent features:

1) The CRLB increases with the noise power.
2) Singularities are observed at $\theta = \pm\pi/2$.

The first feature is intuitive, it states that the theoretical minimum spread of any unbiased estimate worsens as noise power increases. Equivalently, more (Fisher) information is lost as noise power increases. The singularities are a consequence of the '$\cos^2\theta$' term in Eq. (12). They can be justified by observing the encoding structure of the parameter. Recall that

$$\phi_m = (m-1)\pi\sin\theta \implies \theta = \sin^{-1}\left(\frac{\phi_m}{(m-1)\pi}\right).$$

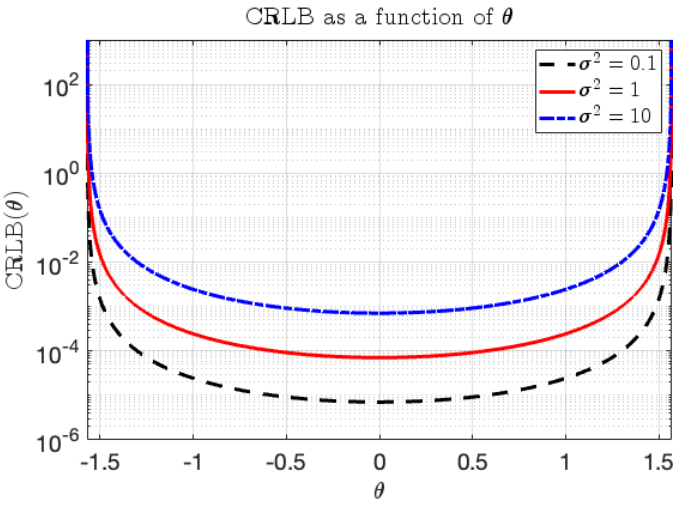

Fig. 2. CRLB as a function of θ for different noise variances ($A_0 = 1$, $N = 10$, $M = 10$, $\omega = 2\pi \times 10^6$, $T_s = 1 \times 10^{-7}$).

The gradient of the function above approaches ∞ as the source angle approaches $\pm\pi/2$. Therefore, slight variances caused by noise when the observed phase is $\pm(m-1)\pi$ (at each element m), would cause large variances in the resultant θ — as observed in Fig. 2 and Eq. (12).

Note, the constants used to obtain the plots in Fig. 2 are used for all of the following plots unless stated otherwise.

III. DOA Estimation with Single-Bit Quantisation

A. Quantised Vector Probability Mass Function

The following section develops the CRLB for case of receiving samples with extreme clipping. The signal model is modified such that each observed sample at each antenna element is quantised as follows,

$$Z_m[n] = \begin{cases} 1, & Y_m[n] > 0 \\ -1, & Y_m[n] \leq 0 \end{cases}. \tag{14}$$

Practically, this is equivalent to implementing 1-bit ADCs at each receiving element. Therefore, the N obtained M-variate random vectors are defined as,

$$\boldsymbol{Z}[n] = \boldsymbol{Q}(\boldsymbol{Y}[n]) \in \mathbb{Z}_{\{-1,1\}}^{M},\ \mathbb{Z}_{\{-1,1\}} = \{-1,1\}. \tag{15}$$

Notice that the $\boldsymbol{Z}[n]$ is now a discrete random vector, and therefore has a probability mass function (PMF). Furthermore, the quantiser is defined element-wise, i.e., per sensor. Therefore, the PMF of $\boldsymbol{Z}[n]$ for a singular n is given by the following joint PMF,

$$\begin{aligned}p(\boldsymbol{z}[n],\theta) &= \mathbb{P}[\boldsymbol{Z}[n] = \boldsymbol{z}[n]]\\ &= \mathbb{P}[Z_1[n] = z_1[n],\ldots,Z_M[n] = z_M[n]].\end{aligned} \tag{16}$$

Note, the underlying noise model remains unchanged, implying

$$Z_i[n] \perp\!\!\!\perp Z_j[n],\ \forall i \neq j.$$

Hence,

$$p(\boldsymbol{z}[n],\theta) = \prod_{m=1}^{M}\mathbb{P}[Z_m[n] = z_m[n]]. \tag{17}$$

Recall, the support for the PMFs in the product term of Eq. (17) is the set $\mathbb{Z}_{\{-1,1\}}$. Thus, $Z_m[n]$ can have the value of 1 with some probability $p_{m,n}$ and -1 with probability $q_{m,n} = 1 - p_{m,n}$. Therefore, each random variable $Z_m[n]$ is a function of a Bernoulli random variable $X \sim \text{Ber}(p_{m,n})$, i.e.,

$$Z_m[n] = 2X - 1. \tag{18}$$

Hence, each PMF in the product term in Eq. (17) can be written as,

$$\mathbb{P}[Z_m[n] = z_m[m]] = p_{m,n}^{\left(\frac{z_m[n]+1}{2}\right)} q_{m,n}^{\left(1-\frac{z_m[n]+1}{2}\right)}. \tag{19}$$

Lastly, the probabilities can be obtained from the following relation between the quantised and non-quantised random variables,

$$\begin{aligned} p_{m,n} &= \mathbb{P}[Z_m[n] = 1] = \mathbb{P}[Y_m[n] > 0] \\ q_{m,n} &= \mathbb{P}[Z_m[n] = -1] = \mathbb{P}[Y_m[n] \leq 0]. \end{aligned} \tag{20}$$

The completed PMF is then given by,

$$\begin{aligned} p(\boldsymbol{z}[n];\theta) = \prod_{m=1}^{M} &\left(1 - \varphi\left(-\frac{x_m[n]}{\sigma}\right)\right)^{\left(\frac{z_m[n]+1}{2}\right)} \\ &\varphi\left(-\frac{x_m[m]}{\sigma}\right)^{\left(1-\frac{z_m n]+1}{2}\right)}. \end{aligned} \tag{21}$$

Here, $\varphi(\cdot)$ represents the standard normal CDF.

B. Log-likelihood Derivation For Quantised Samples

Recall that all N discrete random vectors are independent, with their PMFs given in Eq. (21). Therefore, the likelihood function is the joint PMF of all N random vectors.

$$\begin{aligned} L((\boldsymbol{Z}[n])_{n=1}^{N};\theta) &= \prod_{n=1}^{N} p(\boldsymbol{Z}[n];\theta) \\ &= \prod_{n=1}^{N}\prod_{m=1}^{M} \left(1 - \varphi\left(-\frac{x_m[n]}{\sigma}\right)\right)^{\left(\frac{z_m[n]+1}{2}\right)} \\ &\varphi\left(-\frac{x_m[m]}{\sigma}\right)^{\left(1-\frac{z_m[n]+1}{2}\right)}. \end{aligned} \tag{22}$$

The log-likelihood function is obtained by taking $\ln(\cdot)$ on both sides.

$$\begin{aligned} l((\boldsymbol{Z}[n])_{n=1}^{N};\theta) = &\sum_{n=1}^{N}\sum_{m=1}^{M} \left(\frac{Z_m[n]+1}{2}\right) \\ &\left[\ln\left(1 - \varphi\left(-\frac{x_m[n]}{\sigma}\right)\right) - \ln\left(\varphi\left(-\frac{x_m[n]}{\sigma}\right)\right)\right] \\ &+ \ln\left(\varphi\left(-\frac{x_m[n]}{\sigma}\right)\right). \end{aligned} \tag{23}$$

C. Fisher Information & CRLB

The Fisher information is given by,

$$\mathcal{J}(\theta) = \text{Var}\left[\left(\frac{\partial}{\partial\theta} l\left((\boldsymbol{Z}[n])_{n=1}^{N};\theta\right)\right)\right].$$

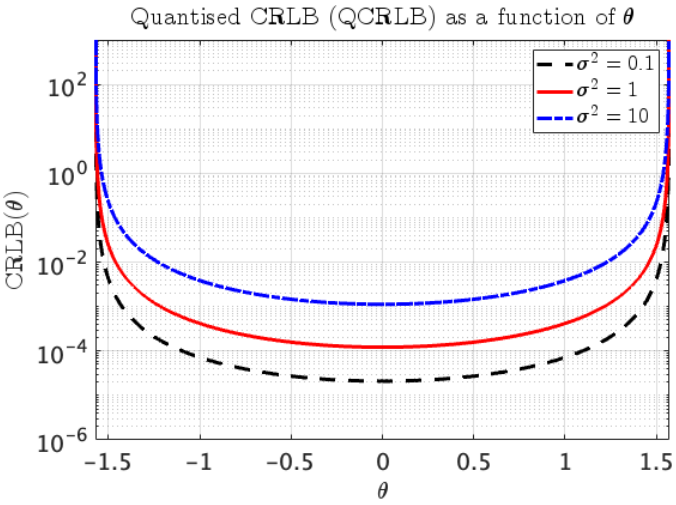

Fig. 3. QCRLB as a function of θ for different noise variances.

As before, each sample $Z_m[n]$ is independent. Therefore, using compact notation, the Fisher information is given by,

$$\begin{aligned} \mathcal{J}(\theta) = &\sum_{n=1}^{N}\sum_{m=1}^{M} \frac{1}{(p_{m,n}q_{m,n})} \\ &\left(g\left(-\frac{x_m[n]}{\sigma}\right)\frac{\partial}{\partial\theta}\left(-\frac{x_m[n]}{\sigma}\right)\right)^2. \end{aligned} \tag{24}$$

Here, $g(\cdot)$ denotes the standard normal PDF and

$$\begin{aligned} \frac{\partial}{\partial\theta}\left(-\frac{x_m[n]}{\sigma}\right) = &\frac{A_0}{\sigma}(m-1)\pi \\ &\sin(\Omega n + (m-1)\pi\sin\theta)\cos\theta. \end{aligned} \tag{25}$$

Subsequently, the CRLB is given by,

$$\text{CRLB}(\theta) = \frac{1}{\mathcal{J}(\theta)}. \tag{26}$$

D. Results & Discussion

The plot in Fig. 3 shows the obtained 'Quantised' CRLB (henceforth referred to as QCRLB) as a function of the parameter θ for different noise variances (noise powers). One can observe that the structure of the plots in Fig. 3 is the same as the 'Non-quantised' CRLB (henceforth referred to as NCRLB). Again, two key difference between the NCRLB and the QCRLB are observed.

1) The QCRLB curves are valued greater than their respective NCRLB curves for all θ, implying a worse theoretical minimum spread of any unbiased estimate.
2) The 'spacing' of the curves for different variances is not as uniform as the NCRLB case, i.e., the separation between the plotted lines increases. This is specifically apparent when observing the curves for $\sigma^2 = 1$ and $\sigma^2 = 10$.

The first observation suggests that quantisation of samples in the presence of noise leads to a greater loss in (Fisher) information, which is intuitive.
To verify the second observation, the NCRLB and QCRLB are plot as functions of decreasing noise variance, i.e., as functions of increasing SNR for a randomly chosen source

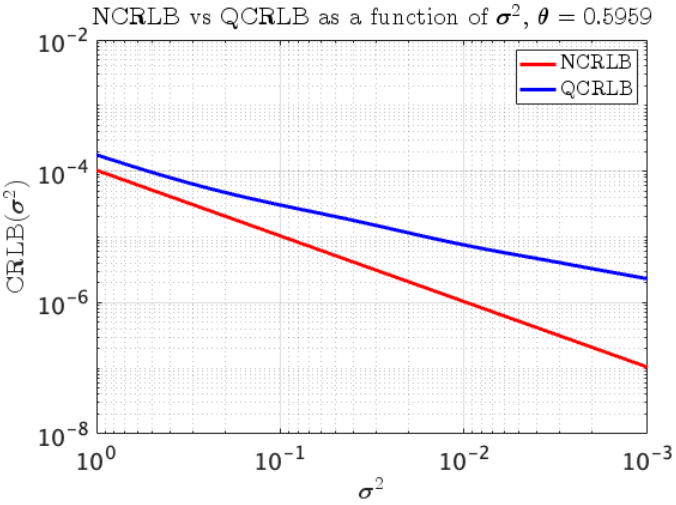

Fig. 4. NCRLB vs. QCRLB as a function of σ^2.

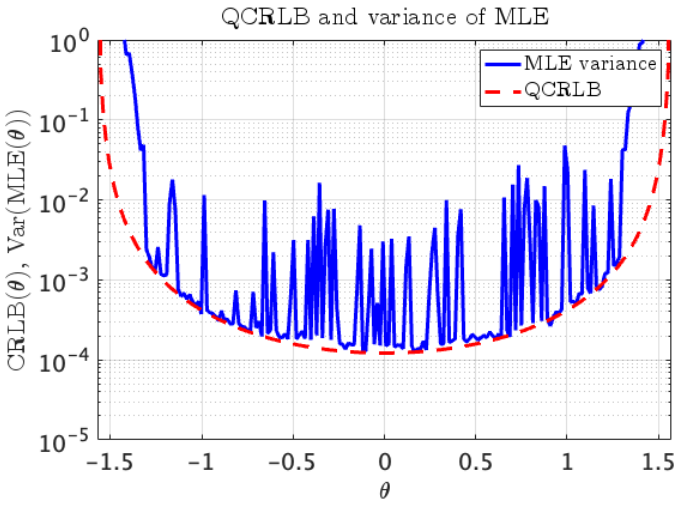

Fig. 5. MLE (Quantised) empirical variance, 200 trials.

angle. As seen from Fig. 4, the separation between the NCRLB and QCRLB increases as the SNR increases. This is an interesting result, suggesting that there is significant loss of information due to quantisation even in the presence of no additive noise. The stated loss of information can be explained by recalling that the signal model temporally samples a continuous cosine signal at each antenna element. Two or more sampled cosine signals can produce the same sampled signal when quantised in the manner defined in Eq. (14). Leading to phase ambiguity and loss of information.

It may be the case that such an increase in separation is not observed when considering a fully continuous signal model. This is attributed to the fact that the amplitude and frequency of the cosine signal are known. Therefore, observing the zero crossings of the quantised continuous wave, one can easily reconstruct the unique cosine source signal. In this scenario, quantisation causes no loss of information in a no-noise environment.

E. Implementing the MLE

A grid-search based MLE was constructed in MATLAB. Fig. 5 compares the resultant empirical variance of the MLE with the QCRLB. As seen from the plot, the MLE variance is bounded by the QCRLB and worse when compared to the non-quantised case. Furthermore, several peaks are observed in Fig. 5 due to a lower angle resolution and the number of conducted trials being limited to 200 in MATLAB to decrease computation time.

IV. Localisation

A. The Localisation Problem

The localisation problem involves determining the position of a signal source within a given space by analysing signals received at multiple observation points. The primary goal is to estimate the spatial coordinates of the signal source. Fig. 6

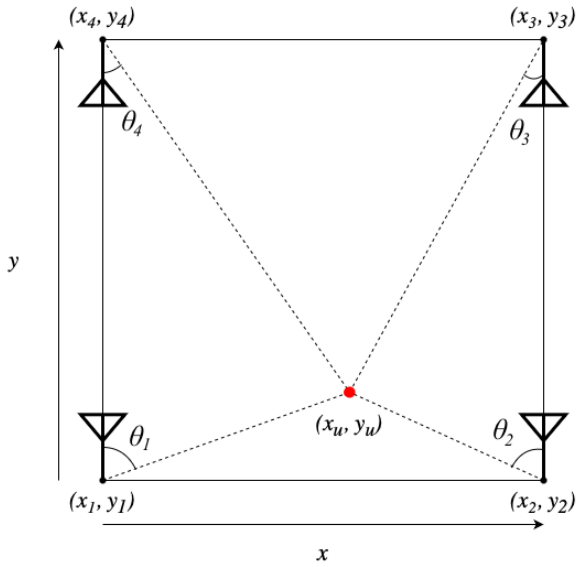

Fig. 6. Model for 2-dimensional localisation.

depicts a scenario in which a signal generated by a source located at (x_u, y_u) is measured at antenna arrays positioned at various locations. To estimate this position in $\mathbb{R}^2$, the following sections outline distinct cases.

B. Two Step Location Estimation

1) Conventional Model: Prior work [1] presents a conventional localisation model that consists of directly receiving angle of arrival estimates. These are defined in [1] as,

$$r_k = \varphi_k + n_k \sim \mathcal{N}(\varphi_k, \sigma_k^2). \tag{27}$$

Here, k indexes the antenna arrays defined in Section IV-A. Each array receives an angle φ, polluted with zero-mean Gaussian noise n, forming the variance of the angle estimate. These received angles originate from (x_u, y_u). Therefore, [1] defines φ_k as,

$$\varphi_m = \tan^{-1}\left(\frac{y_u - y_k}{x_u - x_k}\right) \tag{28}$$

On defining $\boldsymbol{\xi} = (x_u, y_u)$, the PDF of each of the observed estimate k is given by,

$$f(x;\boldsymbol{\xi}) = \frac{1}{\sigma_m\sqrt{2\pi}} \exp\left(-\frac{1}{2}\left(\frac{x - \tan^{-1}\left(\frac{y_u - y_k}{x_u - x_k}\right)}{\sigma_k}\right)^2\right). \tag{29}$$

Assuming independent noise at each array, [1] derives the Fisher information matrix (FIM) (As defined in Appendix A) to be

$$\boldsymbol{\mathcal{J}}(\boldsymbol{\xi}) = \sum_{k=1}^{K} \frac{1}{\sigma_k^2} \frac{1}{\left((y_u - y_k)^2 + (x_u - x_k)^2\right)^2} \begin{bmatrix} (y_u - y_k)^2 & -(y_u - y_k)(x_u - x_k) \\ -(y_u - y_k)(x_u - x_k) & (x_u - x_k)^2 \end{bmatrix}. \tag{30}$$

Therefore, the CRLB is evaluated by inverting the obtained FIM as defined in Eq. (68) in Appendix A. However, Eq. (68) establishes a CRLB for x_u and y_u separately. Therefore, this investigation makes use of the definition in Eq. (72) in Appendix A which provides the CRLB as a function of the complete parameter $\boldsymbol{\xi}$. Therefore,

$$\mathrm{CRLB}(\boldsymbol{\xi}) = \mathrm{tr}(\boldsymbol{\mathcal{J}}(\boldsymbol{\xi})^{-1}). \tag{31}$$

Fig. 7a shows the evaluated 'conventional non-quantised' CRLB (CNCRLB). Note, the parameter being restricted to that square in not a requirement, the CRLB can be calculated for any $(x_u, y_u) \in \mathbb{R}^2$.

2) Using DOA CRLB as Variance of the Estimate: This investigation now derives the localisation CRLB using the obtained DOA estimates in Sections II and III as opposed to assuming angle estimates with an arbitrary variance, received at ambiguous sensors. This shall result in a more practical lower bound for location estimation.

Therefore, the incoming angle of arrival random variables at each array are replaced by DOA estimates of an MLE. As a matter of fact, this choice of estimator proves to be the most convenient. As stated in Appendix A, the MLE possesses an important property of convergence in distribution to a Gaussian. Thus, the PDF of the MLE converges to

$$\mathcal{N}(\theta_k, \mathcal{J}(\theta_k)^{-1}) = \mathcal{N}(\theta_k, \mathrm{CRLB}(\theta_k)). \tag{32}$$

This is particularly convenient as it allows for the use of the existing expression for the FIM.
Eq. (32) implies that the variance of the received estimates is no longer an arbitrary noise variance, but the CRLB of the DOA estimate. Therefore,

$$\sigma_k^2 = \mathrm{CRLB}_{\mathrm{DOA}}(\theta_k) \tag{33}$$

As seen from Eq. (32), the variance of the MLE converges to the DOA CRLB. Therefore, the variance of estimates from the non-quantised scenario converges to the DOA NCRLB and the variance of estimates from the quantised scenario converges to the DOA QCRLB. Figs. 7b and 7c plot the CRLB evaluated in Eq. (31) with $\sigma_k^2 = \mathrm{NCRLB}_{\mathrm{DOA}}$ and $\sigma_k^2 = \mathrm{QCRLB}_{\mathrm{DOA}}$ respectively. It shall be noted that the original angle of arrival model posed no restriction on the received angle sample, however, as defined in Section II, the ULA antenna geometry can only distinguish angles in the range of $(-\pi/2, \pi/2)$. This implies that the positioning of the array shall be chosen in a manner that aligns with the limitations of the ULA. The position conditions for the bounds in Fig. 7 ensure that this angle limitation is never violated. It is important to note that this limitation arises from the chosen array layout in Section II, and is not a general limitation. A different choice in array layout can void this limitation.

On comparing Fig. 7a with Figs. 7b and 7c, two differences can be clearly observed.

1) The bound in Figs. 7b and 7c is significantly higher than that in Fig. 7a for all values of $\boldsymbol{\xi}$.
2) The shape of the surface of the bound in Fig. 7a is considerably different from that in Figs. 7b and 7c.

The first observation is of no true importance. These bounds cannot be numerically compared in a meaningful way. The numerical differences arise only from the difference in variance values of the angle of arrival samples. Fig. 7a has a constant variance from the noise model, and Figs. 7b and 7c have angle dependent variances dependent on the properties of the source signal and the noise affecting it. As seen from Figs. 7b and 7c, a low SNR was used to obtain the DOA CRLB. The differences in the actual shapes of the surfaces imply that the use of practical angle of arrival estimates with their respective variances significantly affect the localisation CRLB.

Proving that this two-step method, using the DOA CRLB to derive the localisation CRLB, yields a true variance lower bound for location estimation using DOA samples, is challenging. Therefore, the following subsection takes inspiration from Section II and [1], to derive the CRLB for direct location estimation from the measured signals and their phase difference.

C. Direct Location Estimation

Consider K distinct antenna arrays with locations (x_k, y_k), as defined in Section IV-A, where each antenna array is a ULA. Theoretically, each ULA may have a different number of elements, however, for simplicity, each ULA is assumed to have M elements. Furthermore, the source signal and the phase function are both adopted from Section II. On comparing with Section II, the central difference is the parameter being the location $\boldsymbol{\xi}$ instead of the angle θ. One can rewrite the angle of arrival at the k^{th} array using insights from [1] as

$$\theta_k = f_k(\boldsymbol{\xi}) = \tan^{-1}\left(\frac{x_u - x_k}{y_u - y_k}\right). \tag{34}$$

For simplicity, let each array k take an equal number of temporal samples N of the incident source. Therefore, each array k receives N M-variate samples.

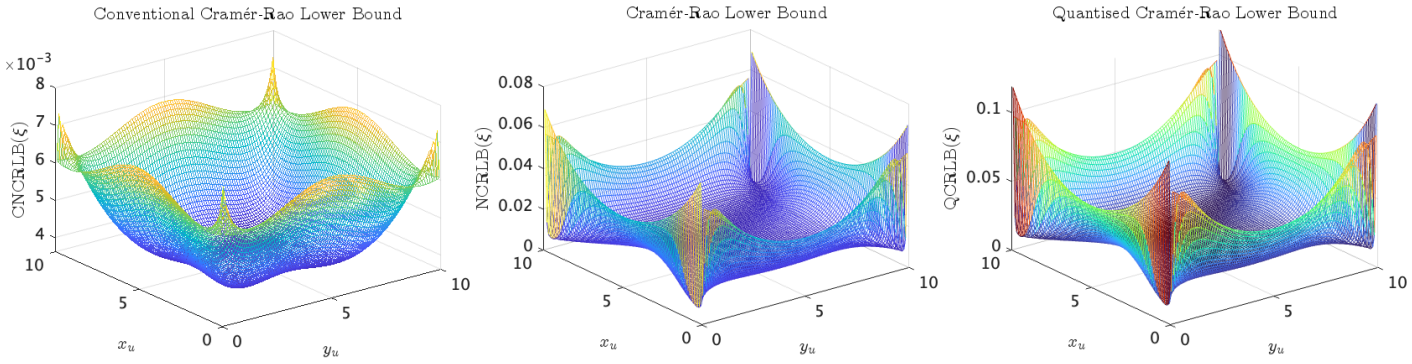

(a) Conventional CRLB, $\sigma_k = 0.00872665$ (b) NCRLB with $\sigma_k^2 = \text{NCRLB}_{\text{DOA}}(\theta_k)$. (c) QCRLB with $\sigma_k^2 = \text{QCRLB}_{\text{DOA}}(\theta_k)$.

Fig. 7. Conventional CRLB and two-step CRLBs evaluated for a 10×10 parameter grid.

1) Non-Quantised: The deterministic signal model for each n and each k is given by,

$$\boldsymbol{x}^k[n] = \begin{bmatrix} A_k \cos(\Omega n + \phi_1(f_k(\boldsymbol{\xi}))) \\ A_k \cos(\Omega n + \phi_2(f_k(\boldsymbol{\xi}))) \\ \vdots \\ A_k \cos(\Omega n + \phi_M(f_k(\boldsymbol{\xi}))) \end{bmatrix}. \tag{35}$$

In order to use the same method of derivation as in Section II, each M-variate sample observed at array k is concatenated into a single tall vector in $\mathbb{R}^{KM}$. Therefore, the revised deterministic signal model for each time sample n is given by

$$\boldsymbol{\mathcal{X}}[n] = \begin{bmatrix} \boldsymbol{x}^1[n] \\ \boldsymbol{x}^2[n] \\ \vdots \\ \boldsymbol{x}^K[n] \end{bmatrix} \in \mathbb{R}^{KM}. \tag{36}$$

As before, the model is completed with the signal polluted with additive random noise. Therefore, the observed samples are given by

$$\boldsymbol{\mathcal{Y}}[n] = \boldsymbol{\mathcal{X}}[n] + \boldsymbol{\mathcal{E}}[n] \in \mathbb{R}^{KM}. \tag{37}$$

Again, $\boldsymbol{\mathcal{E}}$ (AWGN) is assumed to be independent at each element m of each array k. Therefore,

$$\boldsymbol{\mathcal{Y}}[n] \sim \mathcal{N}(\boldsymbol{\mathcal{X}}[n], \boldsymbol{\Sigma}),\ \boldsymbol{\Sigma} = \sigma^2 \mathbb{1} \in \mathbb{R}^{KM \times KM}. \tag{38}$$

The PDF of $\boldsymbol{\mathcal{Y}}$ for a single n is given by,

$$f(\boldsymbol{y}[n]; \boldsymbol{\xi}) = \det(2\pi\boldsymbol{\Sigma})^{-\frac{1}{2}} \exp\left(-\frac{1}{2}\langle \boldsymbol{y}[n] - \boldsymbol{\mathcal{X}}[n], \boldsymbol{\Sigma}^{-1}(\boldsymbol{y}[n] - \boldsymbol{\mathcal{X}}[n])\rangle\right). \tag{39}$$

Considering N independent temporal samples, the likelihood function is given by

$$L((\boldsymbol{\mathcal{Y}}[n])_{n=1}^N; \boldsymbol{\xi}) = \prod_{n=1}^{N} \det(2\pi\boldsymbol{\Sigma})^{-\frac{1}{2}} \exp\left(-\frac{1}{2}\langle \boldsymbol{\mathcal{Y}}[n] - \boldsymbol{\mathcal{X}}[n], \boldsymbol{\Sigma}^{-1}(\boldsymbol{\mathcal{Y}}[n] - \boldsymbol{\mathcal{X}}[n])\rangle\right). \tag{40}$$

Taking $\ln(\cdot)$ on both sides to obtain the log-likelihood function,

$$l((\boldsymbol{\mathcal{Y}}[n])_{n=1}^N; \boldsymbol{\xi}) = N \ln\left(\det(2\pi\boldsymbol{\Sigma})^{-\frac{1}{2}}\right) + \sum_{n=1}^{N} -\frac{1}{2}\langle \boldsymbol{\mathcal{Y}}[n] - \boldsymbol{\mathcal{X}}[n], \boldsymbol{\Sigma}^{-1}(\boldsymbol{\mathcal{Y}}[n] - \boldsymbol{\mathcal{X}}[n])\rangle. \tag{41}$$

As done in Section II, the log-likelihood can be simplified to the following.

$$l((\boldsymbol{\mathcal{Y}}[n])_{n=1}^N; \boldsymbol{\xi}) = -\frac{N}{2}\ln\left(\det(2\pi\boldsymbol{\Sigma})\right) - \frac{1}{2\sigma^2}\sum_{n,m,k}^{N,M,K}\left(Y_m^k[n] - A_k\cos(\Omega n + \phi_m(f_k(\boldsymbol{\xi})))\right)^2. \tag{42}$$

Recall, the FIM is given by

$$\mathbb{R}^{2\times 2} \ni [\boldsymbol{\mathcal{J}}(\boldsymbol{\xi})]_{i,j} = \mathbb{E}\left[\frac{\partial}{\partial\xi_i} l((\boldsymbol{\mathcal{Y}}[n])_{n=1}^N; \boldsymbol{\xi}) \frac{\partial}{\partial\xi_j} l((\boldsymbol{\mathcal{Y}}[n])_{n=1}^N; \boldsymbol{\xi})\right].$$

Computing each component (keeping in mind each $Y_m^k[n]$ is independent),

$$[\boldsymbol{\mathcal{J}}(\boldsymbol{\xi})]_{1,1} = \sum_{n,m,k}^{N,M,K} \frac{(A_k)^2}{\sigma^2} \sin^2\Bigg(\Omega n + (m-1)\pi \sin\left(\tan^{-1}\left(\frac{x_u - x_k}{y_u - y_k}\right)\right)\Bigg)(m-1)^2\pi^2 \cos^2\left(\tan^{-1}\left(\frac{x_u - x_k}{y_u - y_k}\right)\right) \cdot \left[\frac{(y_u - y_k)^2}{[(y_u - y_k)^2 + (x_u - x_k)^2]^2}\right]. \tag{43}$$

$$[\boldsymbol{\mathcal{J}}(\boldsymbol{\xi})]_{2,2} = \sum_{n,m,k}^{N,M,K} \frac{(A_k)^2}{\sigma^2} \sin^2\Bigg(\Omega n + (m-1)\pi \sin\left(\tan^{-1}\left(\frac{x_u - x_k}{y_u - y_k}\right)\right)\Bigg)(m-1)^2\pi^2 \cos^2\left(\tan^{-1}\left(\frac{x_u - x_k}{y_u - y_k}\right)\right) \cdot \left[\frac{(x_u - x_k)^2}{[(y_u - y_k)^2 + (x_u - x_k)^2]^2}\right]. \tag{44}$$

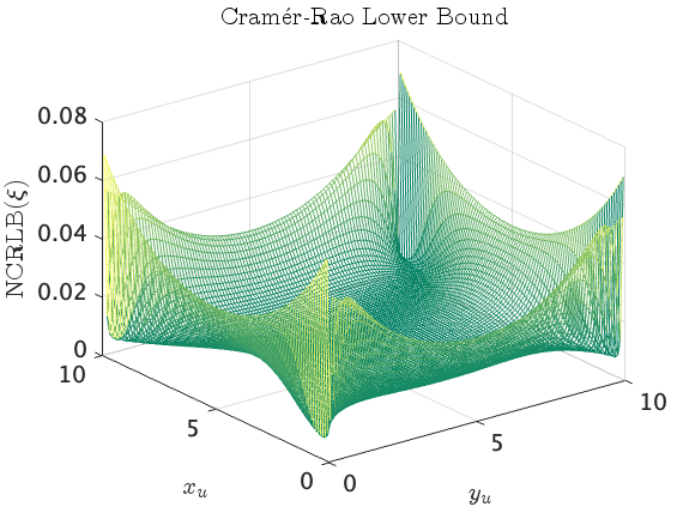

Fig. 8. NCRLB for the parameter restricted to a 10×10 grid.

$$[\boldsymbol{\mathcal{J}}(\boldsymbol{\xi})]_{1,2} = [\boldsymbol{\mathcal{J}}(\boldsymbol{\xi})]_{2,1} = \sum_{n,m,k}^{N,M,K} \frac{(A_k)^2}{\sigma^2} \sin^2\Bigg(\Omega n + (m-1)\pi \sin\left(\tan^{-1}\left(\frac{x_u - x_k}{y_u - y_k}\right)\right)\Bigg)(m-1)^2\pi^2 \cos^2\left(\tan^{-1}\left(\frac{x_u - x_k}{y_u - y_k}\right)\right) \cdot \left[\frac{-(x_u - x_k)(y_u - y_k)}{[(y_u - y_k)^2 + (x_u - x_k)^2]^2}\right]. \tag{45}$$

Consequently, NCRLB is obtained using Eq. (72).

The setup used in the prior subsection and seen in Fig. 6 was used for array positioning, i.e., $K = 4$ and positioned at $(0,0)$, $(10,0)$, $(10,10)$, and $(0,10)$. Fig. 8 presents the obtained NCRLB As seen from Fig. 8, the obtained CRLB for direct location estimation from DOA samples is remarkably similar to the one presented in Fig. 7b. A relative error of the Frobenius norms of the matrices representing the respective CRLBs was computed to be in the orders of magnitude of 10^{-15}. Therefore, the obtained localisation CRLB is essentially the same as the one obtained using the 'two step' method. However, the direct case by definition is the true lower bound on the variance of unbiased estimators of $\boldsymbol{\xi}$.

2) 1-bit Quantisation: The derivation for the bound for quantised samples follows the same approach as in Section III. Assuming an element-wise quantiser for each element of each array, the observed 'tall' discrete random vector is given by:

$$\boldsymbol{\mathcal{Z}}[n] = \begin{bmatrix} \boldsymbol{Z}^1[n] \\ \boldsymbol{Z}^2[n] \\ \vdots \\ \boldsymbol{Z}^K[n] \end{bmatrix} = \begin{bmatrix} Q(\boldsymbol{Y}^1[n]) \\ Q(\boldsymbol{Y}^2[n]) \\ \vdots \\ Q(\boldsymbol{Y}^K[n]) \end{bmatrix}. \tag{46}$$

Therefore, let the PMF be given by:

$$\begin{aligned} p(\boldsymbol{z}[n]) &= \mathbb{P}[\boldsymbol{\mathcal{Z}}[n] = \boldsymbol{z}[n]] \\ &= \mathbb{P}[Z_1^1[n] = z_1^1[n], \ldots, Z_M^1[n] = z_M^1[n], \ldots, \\ &\quad Z_1^K[n] = z_1^K[n], \ldots, Z_M^K[n] = z_M^K[n]]. \end{aligned}$$

As noise remains entirely independent at each array and element, every random variable in the expression above is independent.

$$\therefore \mathbb{P}[\boldsymbol{\mathcal{Z}}[n] = \boldsymbol{z}[n]] = \prod_{k=1}^{K}\prod_{m=1}^{M} \mathbb{P}[Z_m^k[n] = z_m^k[n]]. \tag{47}$$

As seen from Eq. (47), the structure of the 'quantised' PMF remains the same. Each $Z_m^k[n]$ is quantised to ± 1 as done in Section II. Therefore, the complete PMF of the quantised tall vector for any n is given by,

$$\mathbb{P}[\boldsymbol{\mathcal{Z}}[n] = \boldsymbol{z}[n]] = \prod_{k=1}^{K}\prod_{m=1}^{M} p_{n,k,m}^{\left(\frac{z_m^k[n]+1}{2}\right)} q_{n,k,m}^{\left(1-\frac{z_m^k[n]+1}{2}\right)}. \tag{48}$$

with the support of the PMF being $\mathbb{Z}_{\{-1,1\}}$.
Lastly,

$$\begin{aligned} p_{n,k,m} &= \mathbb{P}[Z_m^k[n] = 1] = \mathbb{P}[Y_m^k[n] > 0] \\ q_{n,k,m} &= \mathbb{P}[Z_m^k[n] = -1] = \mathbb{P}[Y_m^k[n] \leq 0]. \end{aligned} \tag{49}$$

Recall all N observed random vectors are independent. Therefore, the likelihood function is constructed using the joint PMF of all N random vectors.

$$\begin{aligned} L((\boldsymbol{\mathcal{Z}}[n])_{n=1}^N; \theta) &= \prod_{n=1}^{N} p(\boldsymbol{\mathcal{Z}}[n]; \theta) \\ &= \prod_{n,k,m}^{N,K,M} \left(1 - \varphi\left(-\frac{x_m^k[n]}{\sigma}\right)\right)^{\left(\frac{z_m^k[n]+1}{2}\right)} \\ &\quad \varphi\left(-\frac{x_m^k[m]}{\sigma}\right)^{\left(1-\frac{z_m^k[n]+1}{2}\right)}. \end{aligned} \tag{50}$$

Here, $\varphi(\cdot)$ represents the standard normal CDF. The log-likelihood function is attained on taking $\ln(\cdot)$ on both sides,

$$\begin{aligned} l((\boldsymbol{\mathcal{Z}}[n])_{n=1}^N; \theta) &= \sum_{n,k,m}^{N,K,M} \left(\frac{Z_m^k[n]+1}{2}\right) \\ &\quad \left[\ln\left(1 - \varphi\left(-\frac{x_m^k[n]}{\sigma}\right)\right) - \ln\left(\varphi\left(-\frac{x_m^k[n]}{\sigma}\right)\right)\right] \\ &\quad + \ln\left(\varphi\left(-\frac{x_m^k[n]}{\sigma}\right)\right). \end{aligned} \tag{51}$$

Each component of the 'quantised' FIM is computed in a manner similar to the 'non-quantised' FIM:

$$\begin{aligned} [\boldsymbol{\mathcal{J}}(\boldsymbol{\xi})]_{1,1} &= \sum_{n,k,m}^{N,K,M} \frac{1}{(p_{n,k,m} q_{n,k,m})} \\ &\quad \left(g\left(-\frac{x_m^k[n]}{\sigma}\right) \frac{\partial}{\partial x_u}\left(-\frac{x_m^k[n]}{\sigma}\right)\right)^2. \end{aligned} \tag{52}$$

$$\begin{aligned} [\boldsymbol{\mathcal{J}}(\boldsymbol{\xi})]_{2,2} &= \sum_{n,k,m}^{N,K,M} \frac{1}{(p_{n,k,m} q_{n,k,m})} \\ &\quad \left(g\left(-\frac{x_m^k[n]}{\sigma}\right) \frac{\partial}{\partial y_u}\left(-\frac{x_m^k[n]}{\sigma}\right)\right)^2. \end{aligned} \tag{53}$$

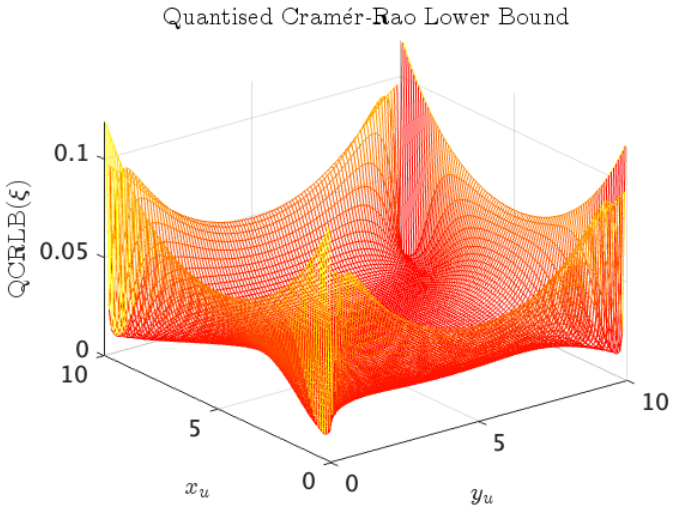

Fig. 9. QCRLB for the parameter restricted to a 10×10 grid.

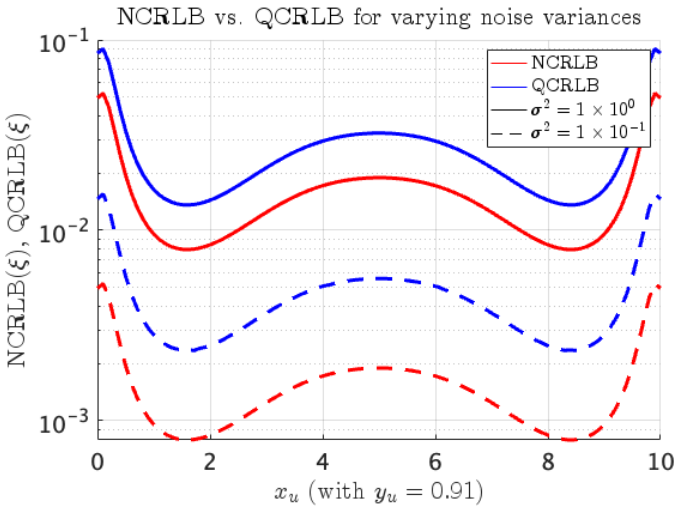

Fig. 10. QCRLB vs. NCRLB for distinct values of noise variance.

$$[\mathcal{J}(\boldsymbol{\xi})]_{1,2} = [\mathcal{J}(\boldsymbol{\xi})]_{2,1} = \sum_{n,k,m}^{N,K,M} \frac{1}{(p_{n,k,m}q_{n,k,m})} g^2\left(-\frac{x_m^k[n]}{\sigma}\right) \frac{\partial}{\partial x_u}\left(-\frac{x_m^k[n]}{\sigma}\right) \frac{\partial}{\partial y_u}\left(-\frac{x_m^k[n]}{\sigma}\right). \tag{54}$$

Here, $g(\cdot)$ denotes the standard normal PDF, and the derivatives are given by

$$\frac{\partial}{\partial x_u}\left(-\frac{x_m^k[n]}{\sigma}\right) = \frac{A_k}{\sigma}\sin\Bigg(\Omega n + (m-1)\pi \sin\left(\tan^{-1}\left(\frac{x_u - x_k}{y_u - y_k}\right)\right)\Bigg)(m-1)\pi\cos\left(\tan^{-1}\left(\frac{x_u - x_k}{y_u - y_k}\right)\right) \cdot \left[\frac{y_u - y_k}{(y_u - y_k)^2 + (x_u - x_k)^2}\right]. \tag{55}$$

and

$$\frac{\partial}{\partial y_u}\left(-\frac{x_m^k[n]}{\sigma}\right) = \frac{A_k}{\sigma}\sin\Bigg(\Omega n + (m-1)\pi \sin\left(\tan^{-1}\left(\frac{x_u - x_k}{y_u - y_k}\right)\right)\Bigg)(m-1)\pi\cos\left(\tan^{-1}\left(\frac{x_u - x_k}{y_u - y_k}\right)\right) \cdot \left[\frac{-(x_u - x_k)}{(y_u - y_k)^2 + (x_u - x_k)^2}\right]. \tag{56}$$

The QCRLB is evaluated using Eq. (72).

Using the same setup as the non-quantised case, Fig. 9 shows the obtained QCRLB. The QCRLB exhibits anticipated behaviour. The obtained lower bound is greater than the NCRLB variant for all parameters $\boldsymbol{\xi}$. This behaviour is made apparent in Fig. 10. In line with the NCRLB, the obtained QCRLB is identical to the one presented in Fig. 7c, with a relative error in the order of magnitude of 10^{-15}. Fig. 10 also shows a familiar observation. The separation between the NCRLB and the QCRLB increases as noise variance decreases (SNR increases). This observation is confirmed in Fig. 11 by plotting the NCRLB and QCRLB as functions of decreasing noise variance for some $\boldsymbol{\xi}$. This increase in separation observed in Fig. 11 is attributed to the deterministic loss of phase information due to quantisation and sampling as discussed in Section II. In addition, the speculation of no loss of information on considering a fully continuous signal model can also be made here.

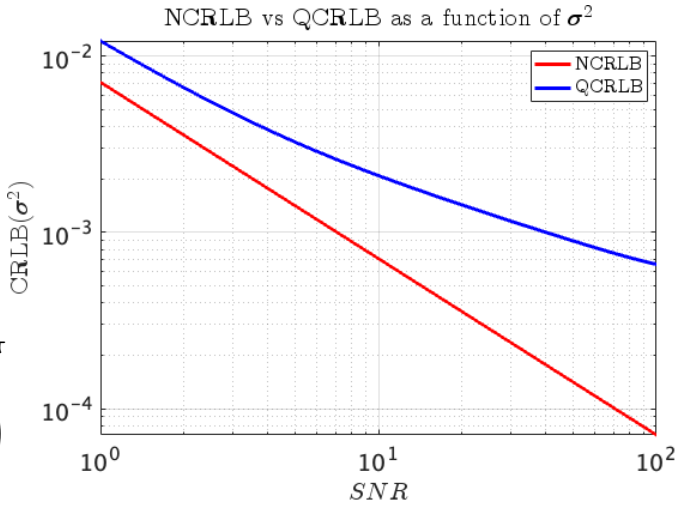

Fig. 11. QCRLB vs. NCRLB for $(x_u, y_u) = (5, 5)$ as a function of (decreasing) noise variance.

V. Conclusion

This thesis began with deriving the CRLB for DOA estimation considering a quantised and non quantised source signal. Here, the two derived bounds were compared and an MLE scheme for the quantised case was implemented. Furthermore, the derived CRLBs were used as variance values of DOA estimates in order to yield more practical,"array aware," localisation CRLBs. The resultant localisation CRLBs were compared to the conventional localisation CRLB that considered zero-mean Gaussian noise added to deterministic DOAs to construct the DOA estimates. Finally, a CRLB for direct location estimation from the measured signals and their

phase differences was derived for the cases of quantised and non-quantised measured signals. A comparison between the bounds was made.
Key results included:

1) The QCRLB for DOA was greater than the NCRLB for DOA for all parameter values. This held true for the 'two-step' localisation bounds as well as the direct localisation bounds, confirming the loss of information due to quantisation in the presence of noise.
2) The CRLB obtained using the 'two-step' approach was identical to the 'direct' derived CRLB for both the quantised and non-quantised case. Implying that the 'two-step' approach is also the true lower bound.
3) As the (SNR increased, the gap between the bounds for quantised and non-quantised scenarios widened for both localisation and DOA estimation. This trend indicates a loss of information even under conditions where no noise is present.

Lastly, there are two applicable improvements in the derivations outlined in Section IV-C that would result in a more practically useful performance bound.

1) Using an 'L'-shaped array instead of a ULA would allow for a complete angular range of $[0, 2\pi]$. This would then allow for unrestricted placement of the antenna arrays in the defined environment. Furthermore, one would be able to freely optimise over array positioning.
2) The model presented in Section IV-C assumes an entirely known signal amplitude for any parameter $\boldsymbol{\xi}$. Furthermore, the derivations and the plots from Section IV-C do not account for the path loss of the signal. As a result, scaling the 10×10 grid has no effect on the bound, rendering it impractical. Instead, allowing for a known initial signal amplitude that varies with the parameter would yield a much more practical bound. This can be achieved with something such as

$$A_k(\boldsymbol{\xi}) = \frac{A_0}{1 + d(\boldsymbol{\xi})}. \tag{57}$$

Here, $d(\boldsymbol{\xi}) = \sqrt{(x_u - x_k)^2 + (y_u - y_k)^2}$

APPENDIX A
BACKGROUND

The foundation of statistical parameter estimation [3] is to obtain information about an underlying population by observing a sample from it. The distribution of this population is assumed to be parameterised by a parameter θ, and thus belongs to a family of distributions defined as

$$\mathcal{P} = \{P_\theta : \theta \in \Theta\}. \tag{58}$$

Here, θ belongs to some subset Θ of a d-dimensional Euclidean space (e.g. $\mathbb{R}^d$). Therefore, the aim of statistical parameter estimation is to observe $X \sim P_\theta$ and estimate θ.

Furthermore, one can interpret observing $X \in \mathbb{R}^N$ as observing N scalar samples $(X[n] \in \mathbb{R})_{n=1}^N$, with P_θ being the joint distribution of the samples. This interpretation allows for the observed sample to be modelled as a received random signal.

A. Estimator Functions

Assuming N random samples $\in \mathbb{R}$, i.e., $(X[n])_{n=1}^N$, with $(x[n])_{n=1}^N$ being the observed realisations of the random samples, one can define an *estimator* function T as

$$(x[1], x[2], \ldots, x[N]) \mapsto T\left(x[1], x[2], \ldots, x[N]\right) \in \mathbb{R}^d. \tag{59}$$

Generally, T can be any function from $\mathbb{R}$ to $\mathbb{R}^d$ (in this example), however, the remainder of this investigation only considers *unbiased* estimators. An estimator T is unbiased if and only if

$$\mathbb{E}\left[T(X[1], X[2], \ldots, X[N])\right] = \theta. \tag{60}$$

1) Maximum Likelihood Estimator (MLE): The MLE is one such function that estimates the parameter by maximising a *likelihood* function, making the observed sample(s) the most probable with respect to the assumed underlying distribution.

Assuming the same N random samples with the joint density or mass function given by $f_N(x[1], \ldots, x[N]; \theta)$, the likelihood function is defined as

$$L(X[1], \ldots, X[N]; \theta) = f_N(X[1], \ldots, X[N]; \theta). \tag{61}$$

Evaluating the likelihood function at the received sample results in a real-valued function of the parameter θ. Maximising the likelihood function with respect to the parameter essentially maximises the density or mass function at the observed sample point, intuitively implying that the observed sample is most probable under the density or mass parameterised by the maximiser. Therefore, one can define the MLE as

$$\hat{\theta} = \arg\max_{\theta \in \Theta} L(X[1], \ldots, X[N]; \theta). \tag{62}$$

Due to convenient properties of the $\ln(\cdot)$ function, this investigation opts to maximise the *log-likelihood* function defined as

$$l(X[1], \ldots, X[N]; \theta) = \ln\left(L_N(X[1], \ldots, X[N]; \theta)\right) \tag{63}$$

instead. The resultant MLE,

$$\hat{\theta} = \arg\max_{\theta \in \Theta} l(X[1], \ldots, X[N]; \theta). \tag{64}$$

is indifferent from the one described in Eq. (62) due to the monotonic nature of the $\ln(\cdot)$ function. The MLE can therefore be obtained by solving the following set of equations,

$$\frac{\partial}{\partial \theta_i} l(X[1], \ldots, X[N]; \theta) = 0, \ \ \forall i \in \{1, \ldots, d\}. \tag{65}$$

B. Fisher Information & CRLB

Multiple unbiased estimators can be constructed to estimate the same parameter. Therefore, a benchmark is necessary to serve as both a performance metric and a theoretical performance limit for all unbiased estimators of that parameter. The Fisher information provides one such performance limit.

The Fisher information quantifies the amount of information that an observed sample carries about the unknown parameter. It provides a measure of the precision with which the

parameter can be estimated. The Fisher information (matrix) is formally defined as

$$[\mathcal{J}(\theta)]_{i,j} = \mathbb{E}\left[\frac{\partial}{\partial\theta_i} l\left((X[n])_{n=1}^{N};\theta\right) \frac{\partial}{\partial\theta_j} l\left((X[n])_{n=1}^{N};\theta\right)\right], \tag{66}$$

or simply

$$\mathcal{J}(\theta) = \mathbb{E}\left[\left(\frac{\partial}{\partial\theta} l\left((X[n])_{n=1}^{N};\theta\right)\right)^2\right] \tag{67}$$

for a scalar parameter.
Using the definition above, a performance limit can be established in the form of an absolute lower bound on the variance of unbiased estimators of θ. This lower bound, known as the ***CRLB***, is stated as follows,

$$\begin{aligned} &[\mathrm{Cov}\left(T((X[n])_{n=1}^{N})\right)]_{k,k} \geq [\mathcal{J}(\theta)^{-1}]_{k,k} \\ \implies &\mathrm{Var}\left(T_k((X[n])_{n=1}^{N})\right) \geq [\mathcal{J}(\theta)^{-1}]_{k,k}. \end{aligned} \tag{68}$$

or simply

$$\mathrm{Var}\left(T((X[n])_{n=1}^{N})\right) \geq \frac{1}{\mathcal{J}(\theta)} \tag{69}$$

for a scalar parameter. Note, that Eq. (68) is a component-wise definition, establishing a CRLB for the estimation of all θ_i separately. This definition of the CRLB can be modified as follows to obtain an expression that is a function of all components of θ. Define $v = T((X[n])_{n=1}^{N}) - \theta$. Therefore,

$$\mathbb{E}[v] = 0 \tag{70}$$

Furthermore,

$$\begin{aligned} \mathbb{E}[v^T v] &= \mathbb{E}[\|v\|^2] \\ &= \mathbb{E}[\mathrm{tr}(v^T v)] \\ &= \mathbb{E}[\mathrm{tr}(vv^T] \\ &= \mathrm{tr}(\mathbb{E}[vv^T]) \\ &= \mathrm{tr}(\mathrm{Cov}(v)), \text{ due to Eq. (70)} \\ &= \mathrm{tr}(\mathrm{Cov}(T((X[n])_{n=1}^{N}))) \end{aligned} \tag{71}$$

On comparing with Eq. (68),

$$\mathrm{tr}(\mathrm{Cov}(T((X[n])_{n=1}^{N}))) \geq \mathrm{tr}(\mathcal{J}(\theta)^{-1}) \tag{72}$$

Lastly, revisiting the discussion on the MLE, an important property to highlight is that the MLE converges in distribution to a Gaussian as $N \to \infty$, i.e.,

$$\sqrt{N}(\hat{\theta} - \theta) \xrightarrow{d} \mathcal{N}\left(0, \mathcal{J}(\theta)^{-1}\right), \tag{73}$$

implying that the MLE attains the CRLB as the sample size N grows.

APPENDIX B
CODE FOR PLOTS

Please find the code to generate all plots within this thesis here https://github.com/shaunakkubal/Localisation-CRLB

REFERENCES

[1] M. Zane, M. Rupp, and S. Schwarz, "Performance investigation of angle of arrival based localization," in *WSA 2020; 24th International ITG Workshop on Smart Antennas*. VDE, 2020, pp. 1–4.

[2] O. Bar-Shalom and A. J. Weiss, "Doa estimation using one-bit quantized measurements," *IEEE Transactions on Aerospace and Electronic Systems*, vol. 38, no. 3, pp. 868–884, 2002.

[3] J. A. Rice and J. A. Rice, *Mathematical statistics and data analysis*. Thomson/Brooks/Cole Belmont, CA, 2007, vol. 371.

[4] P. Stoica, X. Shang, and Y. Cheng, "The cramér–rao bound for signal parameter estimation from quantized data [lecture notes]," *IEEE Signal Processing Magazine*, vol. 39, no. 1, pp. 118–125, 2021.

[5] M. Chen, Q. Li, L. Huang, L. Feng, and M. Rihan, "One-bit cramér–rao bound of direction of arrival estimation for deterministic signals," *IEEE Transactions on Circuits and Systems II: Express Briefs*, 2023.